SCIENCE CHINA
Chemistry

•ARTICLES•

September 2021 Vol.64 No.9: 1504–1509
https://doi.org/10.1007/s11426-021-1036-0

Efficient green OLEDs achieved by a terbium(III) complex with photoluminescent quantum yield close to 100%

Zifeng Zhao[1], Mengying Bian[2], Chenjian Lin[1], Xuzheng Fu[1], Gang Yu[1*], Huibo Wei[3*], Zhiwei Liu[1], Zuqiang Bian[1] & Chunhui Huang[1]

[1]*Beijing National Laboratory for Molecular Sciences, State Key Laboratory of Rare Earth Materials Chemistry and Applications, College of Chemistry and Molecular Engineering, Peking University, Beijing 100871, China;*
[2]*State Key Laboratory for Mesoscopic Physics, Department of Physics, Peking University, Beijing 100871, China;*
[3]*Jiangsu JITRI Molecular Engineering Institute Co., Ltd., Changshu 215500, China*

Received April 29, 2021; accepted May 28, 2021; published online August 20, 2021

Electroluminescence of f-f transition lanthanide complex is a traditional topic for display over decades. Here we report highly efficient organic light-emitting diodes based on a new terbium(III) complex with novel ligand CPMIP (1-(4-cyanophenyl)-3-methyl-4-isobutyryl-pyrazoline-5-one). The high triplet energy level of CPMIP (3.0 eV) and inhibited quenching effects in the solid-state lead to a nearly 100% photoluminescent quantum efficiency of $Tb(CPMIP)_3$. The best $Tb(CPMIP)_3$ device exhibited maximum external quantum efficiency up to 19.7%, setting a new record of OLEDs based on f-f transition lanthanide complexes.

luminescence, terbium, lanthanide complex, organic light-emitting diodes

Citation: Zhao Z, Bian M, Lin C, Fu X, Yu G, Wei H, Liu Z, Bian Z, Huang C. Efficient green OLEDs achieved by a terbium(III) complex with photoluminescent quantum yield close to 100%. *Sci China Chem*, 2021, 64: 1504–1509, https://doi.org/10.1007/s11426-021-1036-0

1 Introduction

Organic light-emitting diodes (OLEDs) with narrowband emission are urgent for next-generation display [1–3] of large color gamut, high contrast ratio and device-flexibility. High efficiency and favorable color purity are both critical for OLED applications [4]. Over decades of efforts, external quantum efficiency (EQE) exceeding 20% in OLED has been demonstrated by phosphorescence [5], thermally activated delayed fluorescence (TADF) [6], and organic radical [7] emitters. Recently, d-f transition lanthanide complex is verified to utilize 100% excitons [8–10] and 20% EQE was achieved in OLEDs [11]. Most of these materials have wide emission spectral bandwidth, thus require special molecular design [12] or incorporated with other dyes [13] to achieve OLEDs with high color-purity. Lanthanide complexes with f-f transition of the central ions have extremely sharp emission bands (in general, <10 nm) [14,15], and their potential in display technology is never off the stage.

Since the efforts of Kido *et al.* [16,17], OLEDs based on f-f transition lanthanide complexes have been studied for over 30 years. Theoretically, The f-f transition lanthanide complexes also have potential to reach 20% EQE in OLEDs [18]. However, till now, the most efficient case is a $Tb(PMIP)_3$-based device with EQE of 15% optimized by better confinement of triplet excitons [19]. The efficiency of f-f transition lanthanide complex device still has the potential to be greatly improved.

High photoluminescent quantum yield (PLQY) of emitter is crucial for achieving highly efficient OLEDs. The suitable triplet energy level and suppressed non-radiative relaxation of ligand are critical for constructing highly efficient luminescent lanthanide complexes [20]. In this work, we present a new ligand CPMIP with a high triplet energy level up to

*Corresponding authors (email: yugang@pku.edu.cn; weihuibo@163.com)

3.0 eV, which could sensitize Tb^{3+} efficiently both in dilute solution and in solid state. Intriguingly, the PLQY of the crystal and doped film is nearly 100%, which is about three times higher than that in dilute solution. Cyano substitute enhanced the thermal stability of $Tb(CPMIP)_3$ by coordination to the adjacent terbium ion without changing the volatility, which is important for fabricating devices by thermal evaporation method. The optimized device based on $Tb(CPMIP)_3$ exhibited a maximum EQE of 19.7%, setting a new record of f-f transition lanthanide complexes based OLEDs.

2 Experimental

2.1 Synthesis of CPMP

4-Cyanophenylhydrazine hydrochloride (2.86 g, 16.8 mmol) was stirred and suspended in ethanol (50 mL), and then 2 M NaOH solution was added dropwise to obtain a yellow solution. Ethyl acetoacetate (2.21 g, 17.0 mmol) was slowly added to the solution obtained in the previous step. 2 M hydrochloric acid was added to the solution to adjust the pH to 4–5, and the mixture was stirred at room temperature for 40 min, then heated to 70 °C and stirred overnight. The solution was then concentrated to 30 mL by reduced pressure distillation, and a large amount of a yellow solid precipitated from the solution. The mixture was filtered and recrystallized from ethanol to give a pale-yellow solid. Finally, 2.27 g 1-(4-cyanophenyl)-3-methyl-pyrazoline-5-one (CPMP) was obtained after vacuum drying at 70 °C. The yield was 67.5%. MS (*m*/*z*, ESI): calcd. 199.1, found 200.1 ($M+H^+$).

2.2 Synthesis of CPMIPH

Under N_2 protection, CPMP (2.23 g, 11.2 mmol) and dry $Ca(OH)_2$ (0.88 g, 11.9 mmol) powder were added to 100 mL of dry 1,4-dioxane and stirred. Then, isobutyryl chloride (1.34 g, 12.6 mmol) was added dropwise to the suspension, and then the solution was refluxed for one hour and then cooled to room temperature. After this mixture was poured into 200 mL of water and the pH was adjusted to neutral with hydrochloric acid, the solids will precipitate directly. The product was filtered and vacuum-dried at 70 °C. 1.33 g white solid CPMIPH was obtained by sublimation purification at 120 °C and 10^{-5} Pa. The yield was 44%. MS (*m*/*z*, ESI): calcd 269.1, found 270.1 ($M+H^+$). ^1H NMR (400 MHz, DMSO-d_6) δ 8.01–7.90 (m, 4H), 3.70–3.55 (m, 1H), 2.44 (s, 3H), 2.09 (s, 1H), 1.03 (d, J = 6.8 Hz, 6H).

2.3 Synthesis of $Tb(CPMIP)_3$

CPMIPH (1.00 g, 3.72 mmol) and NaOH (0.143 g, 3.58 mmol) were added to 10 mL of methanol, and stirred to obtain a clear solution. This solution was heated to 70 °C, and $TbCl_3 \cdot 6H_2O$ (0.462 g, 1.24 mmol) in methanol was added dropwise. Then 10 mL of deionized water was added and white solids precipitated. Maintain the temperature for another 10 min, then cool to room temperature and filter. The solid was washed with a mixed solvent of ethanol/water (1:1) and then dried under vacuum at 70 °C. The sample was then sublimed at 330 °C and 10^{-5} Pa to obtain 0.768 g of white crystalline solid. The yield was 68%. Anal. calcd. for $C_{45}H_{42}N_9O_6Tb$ (found): N: 13.25 (13.08), C: 56.07 (56.08), H: 4.52 (4.39).

2.4 General characterization

Elemental analyses were performed on a VARIO EL analyzer (GmbH, Hanau, Germany). The high-resolution mass spectrum was collected on Bruker Solarix XR FTMS (Germany) by electrospray ionization (ESI) method. UV-visible (UV-Vis) absorption spectra were recorded on a Shimadzu UV-3100 spectrometer (Japan). Fluorescence and transient photoluminescence (PL) decay spectra were measured on an Edinburgh Analytical Instruments FLS980 spectrophotometer (UK). PLQYs were measured on the C9920-02 absolute quantum yield measurement system from Hamamatsu Company (Japan). Thermogravimetric analysis (TGA) and differential scanning calorimetry (DSC) were undertaken with a Q600SDT and Q100DSC instrument (USA), respectively. Cyclic voltammetry was measured in nitrogen-purged CH_2Cl_2 solution at room temperature using a CHI600C voltammetric analyzer and tetrabutylammonium hexafluorophosphate ($TBAPF_6$) (0.1 M) as the supporting electrolyte. The conventional three-electrode configuration consists of a platinum working electrode, a platinum wire auxiliary electrode, and an Ag/AgCl wire pseudoreference electrode.

2.5 OLEDs fabrication and measurement

MoO_3, mCP, DPEPO, TPBi, and LiF were purchased from commercial sources without further purification. DCPPO was synthesized and purified using the method reported in the literature.

The indium tin oxide (ITO) glass substrates were purchased from commercial source. The thickness of the ITO is 80 ± 5 nm, and the sheet resistance is 17–18 Ω per square. The active area of the device is 2.0 mm×2.0 mm. The ITO substrates were ultrasonically cleaned by detergent solution, deionized water, acetone, and ethanol, and dried with N_2 gun before transferred to vacuum chambers. The organic and metal layers were deposited in different vacuum chambers with a deposition rate of around 1 and 1–2 Å s^{-1}, respectively under a base pressure lower than 1×10^{-4} Pa, while the deposition rates of MoO_3 and LiF were roughly 0.1–0.2 Å s^{-1}.

All electric testing and optical measurements were performed under ambient conditions. The EL spectra, *J-V-L*, and EQE characteristics were measured by computer-controlled Keithley 2400 source meter and absolute EQE measurement system (C9920-12) with a photonic multichannel analyzer.

3 Results and discussion

CPMIPH could be effectively synthesized from 4-cyanophenylhydrazine hydrochloride and ethyl acetoacetate, followed by reaction with isobutyryl chloride. $Ln(CPMIP)_3$ could be obtained by CPMIPH and lanthanide chloride hydrate salt ($LnCl_3{\cdot}6H_2O$). The synthetic method for CPMIPH and $Ln(CPMIP)_3$ is shown in Scheme 1.

Crystals of $Ln(CPMIP)_3(EtOH)(H_2O)$ were obtained by slowly evaporating the ethanol/water solution of complexes at room temperature. Due to the large ion radius, lanthanide trivalent ions usually require a high coordination number of 8 or 9 to stabilize the coordination environment. Therefore, additional neutral ligands are needed to satisfy saturated coordination and 3:1 (monoanionic ligands *vs.* Ln^{3+} ions) electrical neutral complexes when bidentate monoanionic ligands were used to construct Ln^{3+} complexes. In this case, an ethanol molecule and a water molecule coordinate to a Ln^{3+} ion as neutral ligands (Figure S1, Supporting Information online). Solvent-free $Ln(CPMIP)_3$ crystals for X-ray analysis were obtained by sublimation of $Ln(CPMIP)_3$-$(EtOH)(H_2O)$ at 300 °C and 10^{-4} Pa. The neutral ligands (EtOH and H_2O) would leave during this process. The structure of $Tb(CPMIP)_3$ was deduced from X-ray diffraction data. As shown in Figure 1, the terbium ions of the complex are seven-coordinated by six oxygen atoms from three bidentate β-diketone ligands and a nitrogen atom from –CN group, forming a binuclear structure. The details of bond length and crystal data were exhibited in Tables S1 and S2 (Supporting Information online).

As demonstrated in Figure 2, the UV-Vis absorption spectrum exhibits a strong absorption band corresponding to the π-π* transition with maxima at 286 nm for $Tb(CPMIP)_3$ ($\varepsilon = 9.18 \times 10^4\ M^{-1}\ cm^{-1}$, where ε is the molar absorption coefficient). The bandgap (E_g), which can be calculated from the onset wavelength of the absorption spectrum, is speculated to be around 3.54 eV (28,600 cm^{-1}). To estimate triplet energy (E_T) value of CPMIP ligand, we obtained the phosphorescent emission spectrum of the $Gd(CPMIP)_3$ with 25 ms delay at 77 K. The E_T was estimated as 3.00 eV (24,150 cm^{-1}), which could be calculated from the first phosphorescent emission peak at 414 nm. The energy gap between E_T (24,150 cm^{-1}) and $^5D_4$ state (20,500 cm^{-1}) of Tb^{3+} ion lies at 3,650 cm^{-1}, which is benefit for energy transfer from ligand to Tb^{3+} ion and inhibiting the reverse energy transfer process. The room temperature emission spectrum of $Tb(CPMIP)_3$ exhibits four strong and sharp emission bands corresponding to the $^5D_4 \rightarrow {}^7F_J$ ($J = 6, 5, 4, 3$)

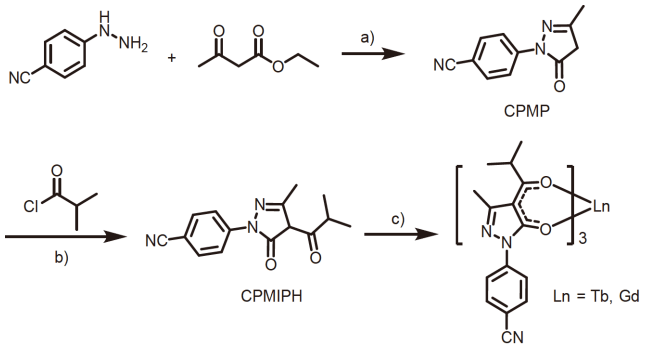

Scheme 1 Syntheses of CPMIPH and $Ln(CPMIP)_3$ complexes. Reaction conditions: (a) ethanol, pH 4–5, 70 °C, over night; (b) $Ca(OH)_2$, dry 1,4-dioxane, reflux, 1 h, under nitrogen; (c) $LnCl_3{\cdot}6H_2O$, NaOH, ethanol/water, reflux.

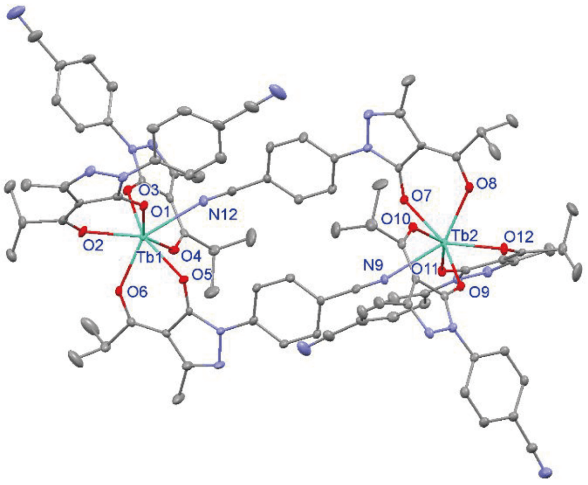

Figure 1 Oak Ridge Thermal Ellipsoid Plot view of the crystal structure of binuclear dimer $[Tb(CPMIP)_3]_2$ at 30% probability level. All hydrogen atoms have been omitted for clarity (color online).

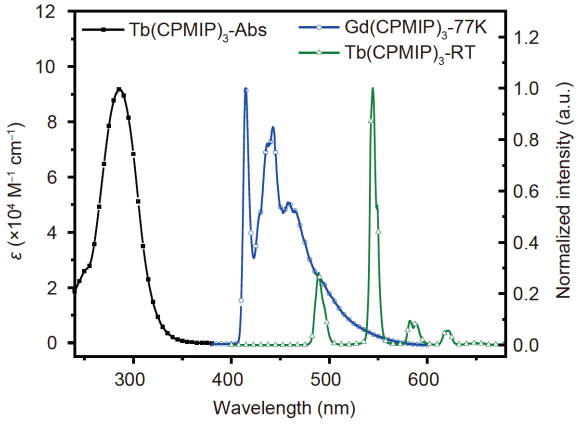

Figure 2 The absorption and emission spectra of $Tb(CPMIP)_3$ at room temperature, and the phosphorescence spectrum of $Gd(CPMIP)_3$ at 77 K. The spectra were recorded in ethanol solution at 10^{-5} M (color online).

transitions with the main peak at 545 nm. The full width at half maxima (FWHM) of the main peak is only 10 nm, which should be ascribed to the shielded f-f transition of lanthanide ions. $Tb(CPMIP)_3$ shows strong emission in both solution and solid-state. Furthermore, the absolute PL quantum efficiencies of $Tb(CPMIP)_3$ were investigated in different states. The data were shown in Table 1. Notably, the PLQY of sublimated crystals could reach 97.1%, while it dramatically decreased to 32.6% when the crystals were dissolved in CH_3OH. It is widely recognized that the O–H vibration would quench the emission of lanthanide ions. Hence deuterated methanol was introduced to replace CH_3OH. The PLQY raised to 48.6% and the emission showed a longer lifetime. It should be attributed to the lower frequency of O–D bond vibration, reducing the quenching effect for lanthanide emission. But the quantum yield in deuterated solution is still only half that of crystals. That implies there is another non-radiative pathway in the complex molecules. The photophysical properties are listed in Table 1.

The thermal properties of the complex $Tb(CPMIP)_3$ were measured by TGA and DSC. The decomposition temperatures (T_d) and the glass transition temperature (T_g) of $Tb(CPMIP)_3$ were observed to be 382 and 156 °C, respectively (Figure S2), which are both higher than that of $Tb(PMIP)_3$. The enhanced thermal stability could be attributed to the increase in molecular weight and the binuclear structure of $Tb(CPMIP)_3$. A high glass transition temperature is desirable for materials in OLEDs because it prevents morphological changes and suppresses the formation of aggregates upon heating.

Cyclic voltammetry was used to evaluate the highest occupied molecular orbital (HOMO) energy level of the complex. The test was conducted in dichloromethane solution using ferrocene (Fc/Fc^+) as an internal reference. Two oxidation peaks were detected during positive scanning (Figure S3). The onset value was adopted for the potential of the irreversible redox peak according to the reference. The HOMO energy level was estimated using the method described by Forrest *et al.* [21]. The lowest unoccupied molecular orbital (LUMO) energy level can be obtained from the HOMO value and the E_g which comes from the UV-Vis absorption spectrum. According to the above methods, the HOMO and LUMO energy levels of $Tb(CPMIP)_3$ were estimated to be −5.7 and −2.2 eV, which could fit most carrier transport and host materials for OLEDs fabrications.

Green OLEDs were fabricated using the terbium complex as the dopant of emitting layers. The base device structure of the OLEDs is ITO/MoO_3 (2 nm)/*m*-bis(*N*-carbazolyl)benzene (mCP):MoO_3 (25 nm, 20 wt%)/mCP (15 nm)/dicarbazolylphenylphosphine oxide (DCPPO):$Tb(CPMIP)_3$ (20 nm, 15 wt%)/bis(2-(diphenylphosphino)phenyl)ether oxide (DPEPO, 10 nm)/1,3,5-tris(*N*-phenylbenzimidazol-2-yl) benzene (TPBi, 30 nm)/LiF (1 nm)/Al (100 nm). The frontier molecular orbital energy levels and triplet energy levels of the materials were shown in Figure 3a. DCPPO was chosen as the host material of the devices because DCPPO possesses bipolar carrier mobility and high triplet energy level up to 3.0 eV [22,23], which is suitable for the host of $Tb(CPMIP)_3$. The film of DCPPO:$Tb(CPMIP)_3$ (15 wt%) shows pure emission from Tb^{3+} ion with 98.9% PLQY, indicating the energy transfer from host to $Tb(CPMIP)_3$ is highly efficient. mCP (E_T = 2.9 eV) and TPBi (E_T = 2.6 eV) serve as the hole and electron transport materials, respectively. The triplet energy level of mCP is slightly lower than that of the host and dopant, and that of TPBi is inadequate for these OLEDs. Neither of them can completely confine triplet excitons in the emitting layer. To solve this problem, a 10 nm thick DPEPO is introduced considering its high triplet energy level (3.1 eV) and relatively weaker electron-transporting ability (compared with TPBi). Additionally, a 20 nm MoO_3 doped mCP was introduced between the MoO_3 and mCP layers to enhance the hole injection and transportation. These methods, on the one hand, make the carrier recombination zone away from the hole transport layer to suppress the diffusion of triplet excitons from emission layer (EML) to mCP. On the other hand, the leakage of triplet excitons from EML to TPBi is inhibited by DPEPO. Moreover, MoO_3 is used as the hole injection layer which modifies the work function of ITO, and LiF is the electron injection layer. The organic molecular structures of these used materials are represented in Figure S4.

For further optimization, the thicknesses of EML and electron transporting layer (ETL) were modified in devices A, B and C. The parameters and performances of the devices are listed in Table 2.

All of the devices exhibit typical Tb^{3+} emission from $Tb(CPMIP)_3$ complex. As an example, Figure 3b depicts the electroluminescence spectra of device C at different vol-

Table 1 Photophysical, electrochemical and thermal analysis data of $Tb(CPMIP)_3$

	E_g [a] (eV)	E_T [b] (eV)	HOMO/LUMO [c] (eV)	PLQY (%)/τ_{obs} (μs)				T_d (°C)	T_g (°C)
				In CH_3OH	In CD_3OD	Crystals	Doped film [d]		
$Tb(CPMIP)_3$	3.54	3.00	−5.7/−2.2	32.6/942	48.6/1289, 1837	97.1/561	98.9/824	382	156

a) Calculated from the absorption edge; b) calculated from the 0-0 transition peak of the phosphorescent spectrum; c) HOMO was obtained by the cyclic voltammetry method, and the LUMO was speculated from the E_g and HOMO energy level; d) doped in DCPPO with 15 wt% concentration.

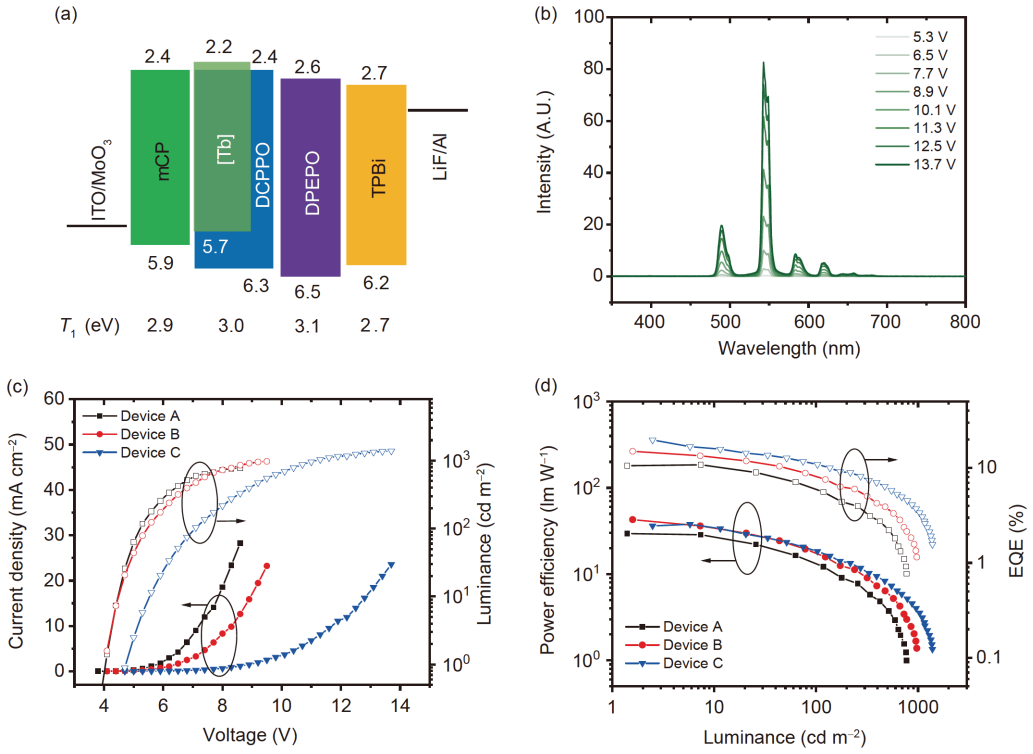

Figure 3 (a) HOMOs, LUMOs and E_T levels of materials in fabricated OLEDs; (b) electroluminescence spectra of device C at different voltages; (c) current density-voltage-luminance (*J*-*V*-*L*) characteristics of the devices; (d) power efficiency-luminance-external quantum efficiency (PE-*L*-EQE) of the devices (color online).

Table 2 The thickness parameters and performances of devices

Devices	Thickness (nm)		V_{on} (V)	EQE (%)		L_{max} (cd m^{-2})	λ_{max} (nm)	CIE (*x*, *y*) @100 cd m^{-2}
	EML	ETL		max	@100 cd m^{-2}			
A	20	30	4.1	10.8	5.6	774	543	0.32, 0.62
B	20	50	4.1	15.0	7.6	971	543	0.32, 0.62
C	40	50	4.7	19.7	10.9	1383	543	0.32, 0.62

tages, indicating the favorable carrier confinement in EML and excellent energy transfer from host to emitter. The current density-voltage-luminance (*J*-*V*-*L*) curves are shown in Figure 3c. The current density and luminance of device A rise fastest among the three devices, indicating device A owns smallest resistance. The maximum EQE and luminance could reach 10.8% and 774 cd m^{-2}, respectively. As the thickness of TPBi increases to 50 nm (Device B), the maximum EQE and luminance increase to 15.0% and 971 cd m^{-2}, respectively, which should be ascribed to the shift of recombination zone away from the mCP layer to reduce the triplet excitons quenching. The relative smaller current density and luminance at the same voltage exhibit larger resistance of device B than that of device A. Considering the long lifetime of lanthanide complexes (millisecond level), the probability of triplet-triplet annihilation and polaron-triplet annihilation is much larger than that of common phosphorescent materials. To further improve device efficiency, the thickness of the emission layer was optimized from 20 to 40 nm in device C. Six devices were fabricated with an average EQE maxima of 18.6% and a highest one of 19.7% (Table S3). The high EQE were achieved by extended recombination zone for reducing triplet exciton annihilation in the emission layer. The maximum luminance of device C is 1383 cd m^{-2}, and the EQE at 100 cd m^{-2} could reach 10.9%, which is the best performance among OLEDs based on f-f transition lanthanide complexes.

Compared with current state-of-the-art performance for green OLEDs with different types of emitters [24–26], our devices show evident disadvantages such as low maximum luminance and serious efficiency roll-off due to the intrinsic millisecond radiation lifetime of f-f transition. The multiple emission bands of Tb^{3+} reduce the color purity of the corresponding OLEDs. These properties are unfavorable for commercial application. However, d-f transition lanthanide

complex can circumvent these issues and open a new stage for future application in OLEDs.

4 Conclusion

In conclusion, nearly 100% PLQY was achieved in a new f-f transition lanthanide complex $Tb(CPMIP)_3$ by rational ligand design. Suitable HOMO and LUMO energy levels and excellent thermal stabilities endow $Tb(CPMIP)_3$ with huge potential in electroluminescence. The EQE of corresponding OLEDs could approach the theoretical limit of 20% by optimizing the device structure carefully. Just like phosphorescence and TADF materials, the f-f transition lanthanide complex was demonstrated as an efficient emitter with 100% exciton utilization efficiency.

Acknowledgements This work was supported by the National Basic Research Program of China (2017YFA0205100), and the Key Project of Science and Technology Plan of Beijing Education Commission (KZ201910028038). Zifeng Zhao acknowledges financial support from the China Postdoctoral Science Foundation (2018M641065, 2021T140009) and BMS-Junior Fellow.

Conflict of interest The authors declare no conflict of interest.

Supporting information The supporting information is available online at http://chem.scichina.com and http://link.springer.com/journal/11426. The supporting materials are published as submitted, without typesetting or editing. The responsibility for scientific accuracy and content remains entirely with the authors.

1 Zhang Q, Li B, Huang S, Nomura H, Tanaka H, Adachi C. *Nat Photon*, 2014, 8: 326–332
2 Tao Y, Yuan K, Chen T, Xu P, Li H, Chen R, Zheng C, Zhang L, Huang W. *Adv Mater*, 2014, 26: 7931–7958
3 Li X, Zhang J, Zhao Z, Wang L, Yang H, Chang Q, Jiang N, Liu Z, Bian Z, Liu W, Lu Z, Huang C. *Adv Mater*, 2018, 30: 1705005
4 Hatakeyama T, Shiren K, Nakajima K, Nomura S, Nakatsuka S, Kinoshita K, Ni J, Ono Y, Ikuta T. *Adv Mater*, 2016, 28: 2777–2781
5 Baldo MA, O'Brien DF, You Y, Shoustikov A, Sibley S, Thompson ME, Forrest SR. *Nature*, 1998, 395: 151–154
6 Uoyama H, Goushi K, Shizu K, Nomura H, Adachi C. *Nature*, 2012, 492: 234–238
7 Ai X, Evans EW, Dong S, Gillett AJ, Guo H, Chen Y, Hele TJH, Friend RH, Li F. *Nature*, 2018, 563: 536–540
8 Wang L, Zhao Z, Zhan G, Fang H, Yang H, Huang T, Zhang Y, Jiang N, Duan L, Liu Z, Bian Z, Lu Z, Huang C. *Light Sci Appl*, 2020, 9: 157
9 Li J, Wang L, Zhao Z, Sun B, Zhan G, Liu H, Bian Z, Liu Z. *Nat Commun*, 2020, 11: 5218
10 Zhan G, Wang L, Zhao Z, Fang P, Bian Z, Liu Z. *Angew Chem Int Ed*, 2020, 59: 19011–19015
11 Zhao Z, Wang L, Zhan G, Liu Z, Bian Z, Huang C. *Natl Sci Rev*, 2021, 8: nwaa193
12 Kondo Y, Yoshiura K, Kitera S, Nishi H, Oda S, Gotoh H, Sasada Y, Yanai M, Hatakeyama T. *Nat Photonics*, 2019, 13: 678–682
13 Shahalizad A, Malinge A, Hu L, Laflamme G, Haeberlé L, Myers DM, Mao J, Skene WG, Kéna-Cohen S. *Adv Funct Mater*, 2021, 31: 2007119
14 Wei H, Zhao Z, Wei C, Yu G, Liu Z, Zhang B, Bian J, Bian Z, Huang C. *Adv Funct Mater*, 2016, 26: 2085–2096
15 Bünzli JCG, Piguet C. *Chem Soc Rev*, 2005, 34: 1048–1077
16 Kido J, Nagai K, Ohashi Y. *Chem Lett*, 1990, 19: 657–660
17 Kido J, Nagai K, Okamoto Y, Skotheim T. *Chem Lett*, 1991, 20: 1267–1270
18 Wang L, Zhao Z, Wei C, Wei H, Liu Z, Bian Z, Huang C. *Adv Opt Mater*, 2019, 7: 1801256
19 Yu G, Ding F, Wei H, Zhao Z, Liu Z, Bian Z, Xiao L, Huang C. *J Mater Chem C*, 2016, 4: 121–125
20 Wei C, Sun B, Cai Z, Zhao Z, Tan Y, Yan W, Wei H, Liu Z, Bian Z, Huang C. *Inorg Chem*, 2018, 57: 7512–7515
21 Dandrade B, Datta S, Forrest S, Djurovich P, Polikarpov E, Thompson M. *Org Electron*, 2005, 6: 11–20
22 Zhao Z, Yu G, Chang Q, Liu X, Liu Y, Wang L, Liu Z, Bian Z, Liu W, Huang C. *J Mater Chem C*, 2017, 5: 7344–7351
23 Tao Y, Xiao J, Zheng C, Zhang Z, Yan M, Chen R, Zhou X, Li H, An Z, Wang Z, Xu H, Huang W. *Angew Chem*, 2013, 125: 10685–10689
24 Ma X, Liang J, Bai F, Ye K, Xu J, Zhu D, Bryce MR. *Eur J Inorg Chem*, 2018, 2018(42): 4614–4621
25 Im Y, Lee JY. *J Inf Display*, 2017, 18: 101–117
26 Lee DR, Kim BS, Lee CW, Im Y, Yook KS, Hwang SH, Lee JY. *ACS Appl Mater Interfaces*, 2015, 7: 9625–9629